Switching Kalman filter for damage estimation in the presence of sensor faults

Neha Aswal, Subhamoy Sen, Laurent Mevel

Switching Kalman Filter for damage estimation in the presence of sensor faults

Neha Aswal[a], Subhamoy Sen[a,*], Laurent Mevel[b]

[a] *Indian Institute of Technology Mandi, Mandi, HP, India*
[b] *Univ. Gustave Eiffel, Inria, Cosys-SII, I4S, Campus de Beaulieu, Rennes, France*

Abstract

Bayesian filtering based approaches for diagnosis of structural damage have been widely employed in structural health monitoring (SHM) research. The approach however may lead to an inaccurate alarm/decision due to the presence of faulty sensor/s. Nevertheless, sensor faults are inevitable during real field SHM in which sensor may malfunction or get detached from the structural surface, registering completely irrelevant information as measurement. Eventually, such erroneous information induce error in the estimation which leads to an inaccurate, sometimes divergent and impractical solution. The current study deals with Bayesian filtering based structural damage detection in the presence of one or multiple (consecutive) sensor faults. The damage detection is addressed with joint state-parameter estimation approach while a switching filtering strategy is employed for sensor fault detection. Switching approach employs multiple possible sensor fault models which are subsequently integrated to the measurement model of the joint estimation approach. The selection of the competent model (/switching between model ensembles) is undertaken recursively based on their likelihood against measured response. The proposed approach is tested on a numerical lumped mass model of a shear frame building, followed by a laboratory experiment on a cantilever beam. It has been perceived that estimation of health for structures measured with faulty sensors can actually lead to a false (positive and negative) alarm which can, however, be avoided by the employment of the proposed approach. The performance of the proposed approach is further established for healthy and damaged system with pre-existing and sudden sensor faults.

1. Introduction

The deterioration of a structure over time has always been a cause of concern. A structure may face a premature member failure due to rusting in reinforcements, water seepage, damage induced by an earthquake, wind and wave, etc. Maintaining large and complex structures within adequate serviceability has therefore become a necessity. To maintain the safety and serviceability or to determine the remaining life of the

*Corresponding author; *E-mail address: subhamoy@iitmandi.ac.in*

structure of interest, monitoring its health, commonly denoted as structural health monitoring (SHM), has therefore become important. To achieve uninterrupted health monitoring, the structure is equipped with a network of sensors in order to collect the response data. Structural health is further interpreted through analysing these responses. Model based SHM approaches have been extensively employed assuming the availability of a sufficiently accurate model, parameterized with a set of location based health parameters or indices (**HI**s). The model-predicted response is then compared to the real measurements in frequency or time domain and the feedback, in terms of prediction error, is employed within a model-updating pipeline to update the model parameters (i.e. **HI**s).

To ensure damage detection in a structure before any catastrophic failure, several SHM approaches have been employed [1] over the last few decades. Vibration based SHM techniques have been very well developed to detect, localize and quantify damage present in the structure. Generally these techniques require sufficiently accurate measurement data (acceleration/strain, etc.) from sensors placed on the structure. Typical deterministic approaches take basis on an idealistic perfect model and clean measurement conditions. However in real-life, measuring the characteristics of a structure faces several uncertainties that originate from unavoidable model inaccuracies, sensor noises, unknown external disturbances, discrepancy in the data recorded by the sensor, etc. Eventually, uncertainties of different kinds and of unknown magnitude creep in the model estimation process to jeopardize the **HI** estimation process. Disregarding the existence of such uncertainties, a deterministic approach is not sufficient to deal with realistic conditions in structural monitoring.

Bayesian filtering provides an efficient approach in this regard, which recursively estimates the parameters in time while handling uncertainties due to model inaccuracies and measurement noise. It should be mentioned here that parameter estimation with Bayesian filtering approach is a nonlinear problem (explained in Section 2), for which a traditional Kalman filtering approach is not applicable. Eventually, for such problems, resorting to nonlinear filter variants (e.g., Extended or Unscented Kalman filter (EKF/UKF), Ensemble Kalman filter (EnKF) and Particle Filter (PF)) becomes imperative. Regardless of the filter variant employed for such problems, there is a need of a sufficiently accurate process and measurement model in order to ensure precision in the estimation. A process model defines the system dynamics through time evolution of a set of unobserved variables, denoted as states. A measurement model further demonstrates the mapping of such hidden states to the corresponding available measurement that can be measured through the sensors. An optimal state estimate eventually necessitates the inaccuracies in these models to be minimal, unbiased and ideally Gaussian so that the error distribution can be modelled through a stationary white Gaussian noise (SWGN) model of known statistics. Thankfully, for most SHM problems, the uncertainties related to the process model due to unknown forcing and subtle model inaccuracies can be modelled using an SWGN model while the measurement noise can also be assumed as a stochastic process of known statistics.

However, sensor faults are inevitable in real field SHM problems which further introduce another kind of

uncertainty in the estimation process and as such can not be modelled through an SWGN model. Typical sensor faults originate due to electronic malfunction and/or detachment of the sensors from the structural surface. Faults are more probable in extreme service conditions. Most filtering-based approaches rely on a predefined measurement model that is invalidated under such conditions. Eventually, for such scenarios, estimating the system parameters by comparing the measurement recorded by a faulty sensor with a non-compatible measurement model can result in a divergence of the filtering solution, causing a false alarm, positive or negative.

This article addresses the aforementioned problem by employing a Switching Extended Kalman filter (SEKF), wherein the system response and health parameters are estimated within a Joint Extended Kalman filter (JEKF) environment. The proposed approach considers a switching strategy based on multiple measurement models (candidates) instead of a single measurement model. The selection of an appropriate measurement model among the possible candidates is done by employing both a switch variable, defined as a Markovian process with a predefined transition probability, and the likelihood of the model prediction. The Switching Kalman filter (SKF) has previously been successfully employed for the Remaining Usable Life (RUL) detection under the assumption of time invariance of the measurement model. This article further extends this approach for systems that are undergoing changes due to both damage and multiple sensor faults. Thereby, the proposed approach ensures the performance of the employed damage detection procedure even in the cases of singular or multiple sensor faults.

The following section discusses the existing knowledge on the topics of SKF based system health estimation and prognosis. Further, the specific application of SKF and its modifications pertinent to health and RUL estimation is discussed. The SKF approach is, then, detailed with its adaption to the proposed SEKF environment. The proposal is numerically tested on an eight degrees of freedom (dofs) lumped mass model of a shear frame building followed by a laboratory experiment on a two-dimensional (2-D) cantilever beam.

2. Literature Review

Bayesian filtering [2–9] has proved its efficiency to accommodate the inherent uncertainties present in modeling real-life SHM problems. This approach defines the system dynamics and the response measurements in a state-space form with the help of two probabilistic models, namely the process (/state propagation) and the measurement (/observation) models. With the process model, the unobserved state is updated over time using a belief propagation strategy, following the Chapman-Kolmogorov equation. Subsequently, the propagated state is observed through the measurement model incorporating the measurement uncertainty. With Bayesian filters, the propagated state estimate is corrected based on the innovation, comparing the predicted measurement with the actual measurement. A recursion of this procedure using the response data received at each sampling instant ensures the state estimation error to be refined in an optimal sense.

To further estimate damage in the structure, health parameters/indices (**HI**s), corresponding to the locations of interest, are defined and incorporated in the so-called augmented state, to be estimated in time alongside the states [10, 11] in a joint state-parameter estimation formulation. However, incorporation of the parameters into the state variables, renders the otherwise linear problem to become a nonlinear one since bi-linear formulation is induced by augmenting parameters in the state vector and the parameters can be estimated through the measurements only by employing a nonlinear mapping (system model, usually a Finite Element model (FEM)).

Typically, for a linear system defined with linear models, Kalman filter (KF) [12] can be considered as a righteous choice for state estimation. However, for nonlinear models where nonlinearity is induced in the process and/or the measurement relations, the application of KF is invalidated. To address nonlinearity in the system model, several modifications in KF have been introduced, such as, EKF [13], UKF [14, 15], EnKF [16] and PF [17]. Focusing on joint state-parameter estimation, JEKF has been established as an efficient method to estimate the state and the augmented health parameters (**HI**s) simultaneously. At the expense of a higher computational cost, this method has been improved upon by decoupling the estimation approaches [7, 18–20], but traditional joint estimation approach is still impelling for handling systems of moderate dimension, because of its excellent computational performance.

The above mentioned methods, although efficient and robust to handle usual model and measurement uncertainties, do not account for anomalies in the measured data due to faulty sensors. SHM may face challenges where a sensor may come off the surface, starts malfunctioning or simply encounters a connection failure. Eventually, for all such cases, the sensors usually either stop recording all together or may register an electrical noise. Consequently, unaware of such discrepancies, an otherwise robust algorithm may fail to estimate the state and the health parameters. An efficient, stand-alone and autonomous SHM algorithm should therefore be designed for localizing and isolating a faulty sensor at its time of occurrence and still continues with the damage estimation, undeterred by the fault. Faulty sensor data may also arise due to the presence of outliers in the measured data, for which outlier probability for detection can be utilized [21, 22]. However present study focuses on faulty measurement data obtained following before-mentioned reasons only.

Several neural network-based sensor fault detection and isolation (FDI) techniques have been developed for application in aerospace engineering as well as structural health monitoring [23]. Most of these studies limit themselves to one faulty sensor at a time. A few methodologies have been able to detect multiple consecutive faults [23] with autonomous detection and isolation [24]. However neural network-based methodologies require large database for training the network. Similar requirements have been observed in statistical hypothesis test model-based sensor fault diagnosis [25]. Detection and isolation of multi-sensor faults have been achieved using null subspace–based approach [26]. Kalman filter has also been employed in a two-step approach, where fault detection has been handled by detecting the change in mean value/variance of the

residuals, and fault isolation is achieved by dual sensor redundancy [27]. However, none of these methods consider the presence of damage in the structure while detecting and isolating faulty sensors.

In this regard SKF [28] can be utilized. SKF defines multiple individual models corresponding to various workability conditions (for example, fault in sensor $1, 2, 3...$ or RUL option $1, 2, 3...$). From the defined models, the model most suitable/close to current situation (i.e., fault in sensor x in reality or RUL x) is then selected by SKF. SKF has been successfully used in condition assessment to predict RUL of various structures [29–31]. The most probable state for each time step is identified by Bayesian estimation [29]. Based on the selected model the predicted remaining useful life varies.

This paper, first, estimates state and parameters (with JEKF), corresponding to all applicable models, where each model corresponds to a scenario of workability of accelerometers with no or single faulty sensor. Further SKF has been used to select the most probable model corresponding to the measurement model with maximum likelihood. The estimated state and health parameters are then chosen accordingly.

3. System model

Typically a state-space model of the system is required to replicate the structural dynamics for Bayesian filtering-based SHM approaches. Moreover, in order to estimate the system health indices in parallel to the states, they need to be integrated within the state-space model. Usually, the physical system is replicated using numerical modeling techniques (e.g. FEM) as an n^{th} order linear time varying (LTV) system with time invariant mass, $\mathbf{M}_{n\times n}$, and time-varying stiffness, $\mathbf{K}(t)_{n\times n}$, and damping, $\mathbf{C}(t)_{n\times n}$, matrices. The non-stationarity in both the stiffness and the damping is due to the time-varying **HI**s, represented with the parameter vector $\boldsymbol{\theta}(t)_{N_\theta\times 1}$. An explicit description of the functional dependence of the system matrices on $\boldsymbol{\theta}(t)$ is however avoided here for the sake of readability.

The governing differential equation for such a system subjected to ambient excitation can be represented as [18, 19],

$$\dot{\mathbf{x}}(t) = \mathbf{F}_c(t)\mathbf{x}(t) + \mathbf{B}_c\mathbf{u}(t) + \mathbf{v}(t) \tag{1}$$

with $\mathbf{F}_c(t) = \begin{bmatrix} \mathbf{0}_{n\times n} & \mathbf{I}_{n\times n} \\ -\mathbf{M}^{-1}\mathbf{K}(t) & -\mathbf{M}^{-1}\mathbf{C}(t) \end{bmatrix}_{2n\times 2n}$ and $\mathbf{B}_c = \begin{bmatrix} \mathbf{0}_{n\times m} \\ \mathbf{M}^{-1}\tau \end{bmatrix}_{2n\times m}$.

$\mathbf{x}(t) = \begin{bmatrix} \mathbf{q}(t) & \dot{\mathbf{q}}(t) \end{bmatrix}^T_{2n\times 1}$, denotes the state variable with $\mathbf{q}(t)$ and $\dot{\mathbf{q}}(t)$ being the displacement and velocity responses, respectively. $\mathbf{0}$ and $\mathbf{I}$ denotes the null and identity matrices, respectively and $\mathbf{u}(t)_{m\times 1}$ represents the ambient force. $\mathbf{v}(t)_{2n\times 1}$ is the process noise accounting for the inherent model inaccuracies. $\tau_{n\times m}$ is a Boolean matrix that maps the effect of $m \times 1$ order input force to $n \times 1$ order dofs. $\mathbf{u}(t)$ and $\mathbf{v}(t)$ can be assumed to have known statistics of SWGN processes with covariance $\mathbf{Q}^u_{m\times m}$ and $\mathbf{Q}^v_{2n\times 2n}$ collectively

inducing the uncertainty in model prediction in the state propagation model. The state variable $\mathbf{x}(t)$ can be mapped to the acceleration measurement $\mathbf{y}(t)$ as

$$\mathbf{y}(t) = \mathfrak{L}\left[\mathbf{H}(t)\mathbf{x}(t) + \mathbf{D}\mathbf{u}(t)\right] + \mathbf{w}(t) \tag{2}$$

$\mathbf{H}(t)_{n\times 2n}$ denotes the LTV measurement model correlating $\mathbf{x}(t)$ to $\mathbf{y}(t)$ while $\mathbf{D}_{n\times m}$ is the direct transmission matrix that maps the impact of $\mathbf{u}(t)$ to $\mathbf{y}(t)$.

$$\begin{aligned} \mathbf{H}(t) &= \begin{bmatrix} -\mathbf{M}^{-1}\mathbf{K}(t) & -\mathbf{M}^{-1}\mathbf{C}(t) \end{bmatrix} \\ \mathbf{D} &= \mathbf{M}^{-1}\tau \end{aligned} \tag{3}$$

Considering only p out of n *dof*s are instrumented with accelerometers, the location matrix $\mathfrak{L}_{p\times n}$ selects the responses from those $p(\subseteq n)$ measured *dof*s and $\mathbf{w}(t)_{p\times 1}$ is the corresponding measurement noise , again assumed as an SWGN process of covariance $\mathbf{R}_{p\times p}$.

The discrete time representation of the above continuous time definition can further be obtained by employing *zero-order-hold* (ZOH) technique [18], with $\mathbf{F}_k$, $\mathbf{B}_k$, $\mathbf{D}_k$, $\mathbf{E}_k$, $\mathbf{H}_k$, $\mathbf{x}_k$, $\mathbf{y}_k$, and $\mathbf{w}_k$, as the discrete time counterparts of the corresponding continuous time entities described above,

$$\begin{aligned} \mathbf{x}_k &= \mathbf{F}_k\mathbf{x}_{k-1} + \mathbf{B}_k\mathbf{u}_k + \mathbf{v}_k; \\ \mathbf{y}_k &= \mathbf{H}_k\mathbf{x}_k + \mathbf{D}_k\mathbf{u}_k + \mathbf{w}_k \end{aligned} \tag{4}$$

$\mathfrak{L}$ has been included within $\mathbf{H}_k$ and $\mathbf{D}_k$ for notational simplicity. The employed time indexing scheme is used as per [7, 32]. The system is defined with the hidden state $\mathbf{x}_k$ and an unknown LTV state propagation matrix $\mathbf{F}_k$. Moreover, a sudden fault in a sensor invalidates the employment of a predefined measurement matrix $\mathbf{H}_k$ throughout the surveillance. In this article, the estimation of LTV $\mathbf{F}_k$ is approached with a joint state-parameter estimation approach (JEKF) in which $\mathbf{F}_k$ is parameterized with $\boldsymbol{\theta}_k$ which are then estimated alongside $\mathbf{x}_k$. For sensor fault detection and isolation, the present study proposes an SKF based approach detailed later in this article.

4. Joint state-parameter estimation

The present study focuses on detecting structural damage in the presence of sensor faults. Eventually, the state propagation matrix $\mathbf{F}_k$ is time varying and therefore needs to be estimated online. Clearly, such problem can be posed as a joint state-parameter estimation problem in which time evolution of certain location-based **HI**s is defined with $\boldsymbol{\theta}_k$ and estimated jointly in time.

With the joint estimation approach, the system is defined with a joint state-space formulation and estimated using traditional filtering approaches, such as EKF [33–35], denoted JEKF. The joint estimation

approach adds up the parameters $\boldsymbol{\theta}_k$ in the vector $\mathbf{x}_k$ to yield a new formalism for the state dynamics, defined with an augmented state vector $\mathbf{X}_k = \{\mathbf{x}_k; \boldsymbol{\theta}_k\}$ of larger dimension. Accordingly, the Chapman-Kolmogorov based belief propagation can be defined as

$$\mathbf{P}(\mathbf{X}_k|\mathbf{y}_{1:k-1}) = \sum_{\mathbf{X}_{k-1}} \mathbf{P}(\mathbf{X}_k|\mathbf{X}_{k-1})\mathbf{P}(\mathbf{X}_{k-1}|\mathbf{y}_{1:k-1}) \tag{5}$$

$\mathbf{X}_{k|k-1}$ is obtained as the mean of such distribution, $\mathbf{E}(\mathbf{X}_k|\mathbf{y}_{1:k-1})$, where $\mathbf{y}_{1:k-1}$ collectively represents all observations including and up to time step $(k-1)$. From Equation (1), the process and input uncertainties for $\mathbf{x}_k$ are known (i.e., $\mathbf{Q}^v$ and $\mathbf{Q}^u$). The same relation for $\boldsymbol{\theta}_k$ requires the associated state transition model to be defined. For this, $\boldsymbol{\theta}_k$ is defined as a random variable and its transition is achieved by adding a perturbation $\mathbf{v}_k^\theta$ at each time step,

$$\theta_k = \theta_{k-1} + \mathbf{v}_k^\theta \tag{6}$$

$\mathbf{v}_k^\theta$ can be safely assumed to follow an SWGN model of covariance $\mathbf{Q}^{\boldsymbol{\theta}}_{N_\theta \times N_\theta}$, where N_θ is the number of parameters. Finally, Equation (5) can be represented through an algebraic equation,

$$\mathbf{X}_k = \mathcal{F}_k(\mathbf{X}_{k-1}) + \mathcal{B}_k\mathbf{u}_k + \mathbf{v}_k^{\mathbf{X}}; \tag{7}$$

where $\mathcal{F}_k(\mathbf{X}_{k-1})$ defines the new nonlinear state transition function for both response as well as parameter states. The input matrix $\mathcal{B}_k$ can be obtained as $\mathcal{B}_k = \begin{bmatrix} \mathbf{B}_k \\ \mathbf{0} \end{bmatrix}$. The covariances of the overall process noise, $\mathbf{v}_k^X$, and the overall input noise can be obtained as, $\mathcal{Q}^{\mathbf{X}} = \begin{bmatrix} \mathbf{Q}^{\mathbf{v}} & \mathbf{0} \\ \mathbf{0} & \mathbf{Q}^{\boldsymbol{\theta}} \end{bmatrix}$ and $\mathcal{Q} = \begin{bmatrix} \mathbf{Q}^{\mathbf{u}} & \mathbf{0} \\ \mathbf{0} & \mathbf{Q}^{\boldsymbol{\theta}} \end{bmatrix}$, respectively. The prior estimate (i.e.,$\mathbf{X}_{k|k-1}$)[1] can be further be updated to the corresponding posterior (i.e., $\mathbf{X}_{k|k}$), using the Bayesian approach conditioned on the current measurement data, i.e., $\mathbf{y}_k$, as

$$\mathbf{P}(\mathbf{X}_k|\mathbf{y}_{1:k}) \propto \mathbf{P}(\mathbf{y}_k|\mathbf{X}_k)\mathbf{P}(\mathbf{X}_k|\mathbf{y}_{1:k-1}) \tag{8}$$

where $\mathbf{X}_{k|k}$ is obtained as its mean. The data likelihood $\mathbf{P}(\mathbf{y}_k|\mathbf{X}_k)$ however needs a mapping of the estimated states to the corresponding measurements (i.e., a measurement model). For a linear system, the mapping of $\mathbf{x}_k$ is straight forward, while $\boldsymbol{\theta}_k$ requires a nonlinear mapping (typically with an FE model) forcing the measurement model to be nonlinear.

$$\tilde{\mathbf{y}}_k = \mathcal{H}_k(\mathbf{X}_k) + \mathbf{D}_k\mathbf{u}_k + \mathbf{w}_k \tag{9}$$

[1]An estimate $x_{i|j}$ denotes the estimate for random variable x at i^{th} time instant using information including and up to j^{th} time instant along the sample path $\mathbf{y}_{1:k}$.

Upon mapping the states to the predicted measurements $\tilde{\mathbf{y}}_k$, the data likelihood can be obtained using a likelihood function with the departure of prediction from the real measurement $\mathbf{y}_k$ as its argument.

EKF has been efficiently employed with such joint estimation modeling for several joint state-parameter estimation problems (JEKF). In these approaches, the nonlinear state and measurement functions are replaced with the corresponding Jacobians around the current state estimates obtained through a first order Taylor series expansion. It should be acknowledged here that despite its wide spread application as a parameter estimator, JEKF has also been criticized for not having a required analytical form and for not being ergodic [36]. JEKF has often been observed to cause divergence in the solution owing to the increased dimension in the state variables [37]. Still, JEKF has been established as the cheapest nonlinear estimator, in terms of computational cost, for moderate-size systems and its wide application also supports its use for systems that are not strongly nonlinear. With prompt detection of structural faults in our focus, JEKF therefore can be identified as an efficient candidate that can localize and quantify structural damage quickly at a reduced computational effort. However, other Bayesian estimation and monitoring approaches can replace JEKF, which will not hurt the applicability of the switching method proposed in this article.

5. SKF approach

With the system estimation framework defined in Section 4, the system model should either be parameterized and estimated along with state or have several filters to compute with the different system models. However, the model can not always be parameterized correctly, especially for cases where sudden changes have to be considered. For the current study, due to the possibility of a sensor fault, the measurement model may change abruptly and this change may be difficult to track through parameterization of the system model, if the tracking is done through some adaptive algorithm. Eventually, one needs to employ several acceptable measurement models in parallel which will lead to an exponential growth in the belief state, in the order of n^t, where t is the number of steps.

In this endeavor, SKF can be considered to address detecting and isolating sensor faults in the presence of the usual system model inaccuracies and measurement uncertainties due to sensor noises. Like any other typical Bayesian filter, SKF can also be posed as a Dynamic Bayesian Network with multiple possible system models at each time instant. For each of the system model candidates, a dedicated state estimator (say Kalman filter) can be employed. In the current paper, where sensor fault is considered, the models differ by the measurement modeling. The different models are $\{\mathcal{S}^{m_i};\ m_i = 1, 2, \cdots, m\}$, where m denotes the number of measurement model possible, which of course depends on the assumption on maximum possible sensor faults (d_s) out of p sensors as $m = \sum_{i=0}^{d_s} C_i^p$. At each time step, the current model belongs to this model set. An additional discrete Markovian variable S_k, termed as switch, is employed to describe the current model at a particular time instant k. Accordingly, S_k is a discrete random variable with values in $(1, 2, \cdots, m)$. It denotes the index of the measurement model at time instant k.

Eventually, in each time step, the switch can be positioned at any arbitrary measurement model (say i) with n_o options for transition to another measurement model (say j). The stationary transition probability corresponding to transition from the i^{th} model, at time instant $(k-1)$, to the j^{th} model, at time instant k, is denoted as $\mathbf{Z}^{ij}$. The current study focuses on sensor fault detection and the switch is employed to select among the possible measurement models while the state propagation model is assumed as an LTV model and its estimation is dealt separately with the JEKF approach detailed in Section 4. Notice that a variation in the model parameter values due to damage does not change S_k, only a sensor fault can. The challenge for the algorithm is to discriminate between sensor faults and damage.

Eventually, for such system definition, the objective is to estimate the model switch probability for an ensemble of measurement models and thereby enabling the measurement/state propagation modeling to switch between different sensor fault conditions. With JEKF in force, the linearized system equation can be represented as

$$\begin{aligned} \mathbf{X}_k &= \bar{\mathcal{F}}_k \mathbf{X}_{k-1} + \mathcal{B}_k \mathbf{u}_k + \mathbf{v}_k^{\mathbf{X}} \\ \tilde{\mathbf{y}}_k &= \bar{\mathcal{H}}_k^j \mathbf{X}_k + \mathbf{D}_k^j \mathbf{u}_k + \mathbf{w}_k^j \end{aligned} \tag{10}$$

$\bar{\mathcal{F}}_k$ and $\bar{\mathcal{H}}_k$ denote the locally linearized state transition and measurement models. Superscript j in $\bar{\mathcal{H}}_k^j$ associates the notation to the j^{th} measurement model and $\mathbf{D}_k^j$ is the associated direct transmission matrix. $\mathbf{w}_k^j$ is a realization from an SWGN process modeling the measurement noise for the j^{th} noise model and assumed to be an SWGN process of covariance $\mathbf{R}^j$. Additionally, S_k^{ij} defines the probability of the model to be $\mathcal{S}^i$ at time instant $(k-1)$ and to be $\mathcal{S}^j$ at time instant k, given the state of observations $\mathbf{y}_{1:k}$.

For each j^{th} model ($j \in (1, \cdots, n_o)$), a standalone state filter can be employed to propagate and update the prior estimate obtained from i^{th} filter ($i \in (1, \cdots, n_o)$), thereby resulting in n_o filters running in parallel: the covariance $\mathbf{P}_{k|k}$ (resp. $\mathbf{P}_{k|k-1}$) is the variance of the state estimate given the observations $\mathbf{y}_{1:k}$ (resp. $\mathbf{y}_{1:k-1}$) [38]. For i^{th} filter, the prior estimates for $\mathbf{X}_{k-1|k-1}^i$ and $\mathbf{P}_{k-1|k-1}^i$ can be evolved in time and later observed through the j^{th} model as

$$\begin{aligned} &\text{State propagation} && \mathbf{X}_{k|k-1}^i = \bar{\mathcal{F}}_k \mathbf{X}_{k-1|k-1}^i \\ &\text{Covariance propagation} && \mathbf{P}_{k|k-1}^i = \bar{\mathcal{F}}_k \mathbf{P}_{k-1|k-1}^i \bar{\mathcal{F}}_k^T + \mathcal{B}_k \mathcal{Q}^{\mathbf{X}} \mathcal{B}_k^T + \mathcal{Q} \\ &\text{Innovation} && \mathbf{i}_k^{ij} = \mathbf{y}_k - \bar{\mathcal{H}}_k^j \mathbf{X}_{k|k-1}^i \end{aligned} \tag{11}$$

In the following, the state estimates can be updated considering correlated noise in process and measurement model as

$$\begin{aligned} &\text{Kalman gain} && \mathbf{K}^{ij} = (\mathbf{P}_{k|k-1}^i \bar{\mathcal{H}}_k^{j\,T} + \mathcal{B}_k \mathcal{Q}^{\mathbf{X}} \mathbf{D}_k^{j\,T}) \mathcal{J}_k^{j\,-1} \\ &\text{State update} && \mathbf{X}_{k|k}^{ij} = \mathbf{X}_{k|k-1}^i + \mathbf{K}^{ij} \mathbf{i}_k^{ij} \\ &\text{Covariance update} && \mathbf{P}_{k|k}^{ij} = (\mathbf{I} - \mathbf{K}^{ij} \bar{\mathcal{H}}_k^j) \mathbf{P}_{k|k-1}^i \end{aligned} \tag{12}$$

where, innovation error covariance, $\mathcal{J}_k^j = \bar{\mathcal{H}}_k^j \mathbf{P}_{k|k-1}^i \bar{\mathcal{H}}_k^{j\,T} + \mathbf{D}_k^j \mathcal{Q}^{\mathbf{X}} \mathcal{B}_k^T \bar{\mathcal{H}}_k^{j\,T} + \bar{\mathcal{H}}_k^j \mathcal{B}_k \mathcal{Q}^{\mathbf{X}} \mathbf{D}_k^{j\,T} + \mathbf{D}_k^j \mathcal{Q}^{\mathbf{X}} \mathbf{D}_k^{j\,T} + \mathbf{R}_k^j$.

Subsequently, the estimates obtained from all the filters under different possible model transition scenarios have to be weighted and combined. The switch variable, in this regard, helps to obtain a weighted sum of the posterior estimates for state and covariance based on their individual likelihood $\mathbf{L}_k^{ij}$, that can be obtained as:

$$\mathbf{L}_k^{ij} = |\mathbf{G}_k^{ij}|^{-0.5} \exp^{-0.5 \delta_k^{ij} \mathbf{G}_k^{ij\,-1} \delta_k^{ij\,T}} \tag{13}$$

with $\delta_k^{ij} = \mathbf{y}_k - \bar{\mathcal{H}}_k^j \mathbf{X}_{k|k}^{ij}$ and $\mathbf{G}_k^{ij} = \bar{\mathcal{H}}_k^j \mathbf{P}_{k|k}^{ij} \bar{\mathcal{H}}_k^{j\,T} + \mathbf{R}^j$ being the residual error and its covariance estimate, respectively, for the model transition scenario from i^{th} to j^{th} measurement model. In that sense the n_o values of j span a subset of the whole model collection depending on the current model i.

The probability of the model to switch from i^{th} to j^{th} model, i.e., S_k^{ij}, can be obtained using a predefined (and time invariant) transition probability $\mathbf{Z}^{ij}$, and the likelihood estimate $\mathbf{L}_k^{ij}$. Each element in the transition probability matrix $\mathbf{Z}^{ij}$ signifies that the model switches between i and j as defined by the user. S_k^{ij} can be obtained for all $\{ij\}$[2]

$$S_k^{ij} = \mathbf{P}(S_k = j | \mathbf{y}_{1:k} \text{ and } S_{k-1} = i) = \frac{\mathbf{L}_k^{ij} \mathbf{Z}^{ij}}{\sum_{j=1}^{n_o} \mathbf{L}_k^{ij} \mathbf{Z}^{ij}} \tag{14}$$

Corresponding to the state transition from any of the $\mathcal{S}^i$s to $\mathcal{S}^j$, $\mathbf{X}_{k|k}^{ij}$ denotes the corresponding posterior estimates in which measurement model j has been employed. There are n_o state estimates $\{\mathbf{X}_k^{ij}; j = 1, \cdots, n_o\}$ with their individual normalized weights w^{ij} as S_k^{ij}.

Using this collection of weights (w^{ij}), eventually, for the a priori measurement model i, the weighted estimate for the state can be obtained as:

$$\hat{\mathbf{X}}_{k|k}^i = \sum_{j=1}^{n_o} w_k^{ij} \mathbf{X}_{k|k}^{ij} \tag{15}$$

Subsequently, for each state estimator, the state error covariance associated to $\hat{\mathbf{X}}_{k|k}^i$ can be defined as:

$$\begin{aligned} \hat{\mathbf{P}}_{k|k}^i &= \mathbf{cov}_{|\mathbf{y}_{1:k}}(\hat{\mathbf{X}}_{k|k}^i - \mathbf{X}_k) \\ &= \textstyle\sum_{j=1}^{n_o} w_k^{ij} \{ \mathbf{cov}_{|\mathbf{y}_{1:k}}(\mathbf{X}_{k|k}^{ij} - \mathbf{X}_k) + \mathbf{cov}_{|\mathbf{y}_{1:k}}(\hat{\mathbf{X}}_{k|k}^i - \mathbf{X}_{k|k}^{ij}) + 2\mathbf{E}\left[(\mathbf{X}_{k|k}^{ij} - \mathbf{X}_k)(\hat{\mathbf{X}}_{k|k}^i - \mathbf{X}_{k|k}^{ij})^T | \mathbf{y}_{1:k}) \right] \} \\ &= \textstyle\sum_{j=1}^{n_o} w_k^{ij} (\mathbf{P}_{k|k}^{ij} + \epsilon_k^{ij} \epsilon_k^{ij\,T}) + 2\mathbf{E}\left[(\mathbf{X}_{k|k}^{ij} - \mathbf{X}_k) | \mathbf{y}_{1:k} \right] (\hat{\mathbf{X}}_{k|k}^i - \mathbf{X}_{k|k}^{ij})^T \end{aligned} \tag{16}$$

where the residual error $\epsilon_k^{ij} = \hat{\mathbf{X}}_{k|k}^i - \mathbf{X}_{k|k}^{ij}$ is the departure of $\{\mathbf{X}_k^{ij}; i = 1, \cdots, n_o\}$ from the corresponding weighted sum, i.e., $\hat{\mathbf{X}}_{k|k}^i$. $\mathbf{X}_{k|k}^{ij}$ being the optimal unbiased estimate for $\mathbf{X}_k$, the expectation of the departure is ideally zero. Finally, the residual error covariance for k^{th} time step can be obtained as:

[2] $\{ij\}$ is a list of all possible transitions at a given time step, in accordance to the decision tree (cf. Figure 1, Section 5.1) denoting transition between i^{th} and j^{th} measurement models.

$$\hat{\mathbf{P}}^{i}_{k|k} = \sum_{j=1}^{n_o} w^{ij}_k (\mathbf{P}^{ij}_{k|k} + \epsilon^{ij}_k \epsilon^{ijT}_k) \tag{17}$$

5.1. Candidate measurement model selection

In this section, the adopted measurement model and assumed transition probability between one model to another has been detailed. Assuming p ($p \leq n$) dofs are instrumented with sensors, m measurement models are defined to be possible. The possible model number is however conditioned on the assumption on possible sensor faults being detected by the algorithm . In this study, a maximum of two sensor faults are considered. Under each sensor fault condition, the next possible sensor fault models can be formulated using a decision tree as given in Figure 1.

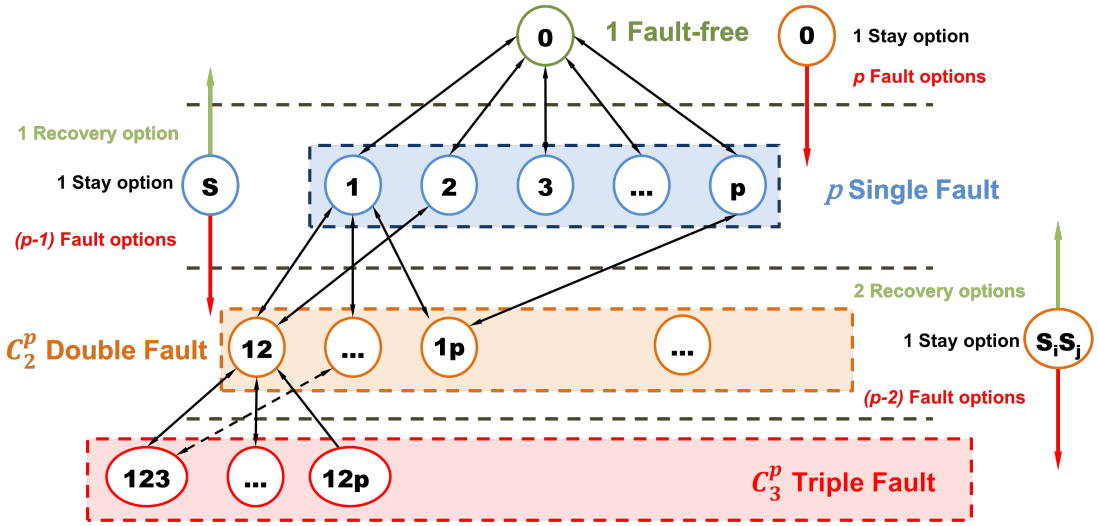

Figure 1: Model transition tree schematic

Evidently, each candidate model is defined with the sensor working states (i.e. working (1) or faulty (0)) with three transition possibilities: 1. the system continues with the same fault model (Stay), 2. get induced with one more sensor fault (Fault Progression) and lastly, 3. a faulty sensor starts working again. The last scenario is obviously rare but still needs consideration in the model ensemble to appreciate the minuscule transition probability for a sensor to be working again. This option also allows to compensate for false alarms allowing the algorithm to return to a steady state after a wrongly assumed false alarm. Clearly, with this renewed definition for the candidate models, the ensemble becomes capable of capturing a multi-sensor fault scenario.

Accordingly, the starting model can be assumed to be fault free, meaning all sensors are working fine. This model got $(p + 1)$ options for model transition: 1 option to stay or move to p possible sensor fault situation (Fault Progression) involving fault at a particular sensor. It has however been assumed that no

two sensors are getting faulty or repaired at the same instant during the estimation. However it no way restricts those faults to occur simultaneously in reality. This strategy is adopted to simplify the estimation process. On premise of this assumption, only one fault-free and p single fault models are possible. With a fault already confirmed, each of the p single fault model has therefore one option to stay, $(p-1)$ options to get induced to another fault in the remaining $(p-1)$ working sensors or a minuscule probability of getting repaired. Recall that C_2^p denotes the number of possible combination with 2 out of p sensors. Eventually, there can be a total number of C_2^p possible fault models, with each having again one stay, two repair, and $(p-2)$ fault progression options.

To elaborate the candidate models further, the fault models pertinent to a simple three sensor system can be explained. Given that, the estimation will be considering maximum of two faulty sensors, the possible models are 1. all sensors working, 2. three single fault models with faults at $1/2/3^{rd}$ sensor, 3. three double fault scenarios with faults at $(1-2)/(2-3)/(3-1)$ sensors. Note that with three fault condition no relevant information is available from which the system can be estimated. However for a sensor network with more sensors, three or more sensor fault models can always be considered. Following the same strategy detailed before, the ensemble can be bigger with consideration of three fault sensor as well. The possible model transition will follow the path as given in the decision tree (or fault propagation tree) which will clearly prevent a fault model of double fault at sensors 3 and 1 to transit to no fault or single fault at 2, but surely allow to have options like single fault at 3 or 1 or moving to triple fault at 1, 2 and 3.

Among these, the first model ($\mathcal{S}^1$ of order $1 \times p$) denotes a no-fault condition in which each of the sensors is intact and working perfectly while the remaining models denote a sensor-fault scenario involving one or two sensor faults. Eventually the model ensemble can be represented as,

$$\begin{aligned} \mathcal{S} &= \left[\mathcal{S}^1;\ \mathcal{S}^2;\ \mathcal{S}^3;\ \cdots;\ \mathcal{S}^m\right]_{(1+p+C_2^p)\times p} \\ &= \begin{bmatrix} 1 & 1 & 1 & \cdots & 1 & 1 \\ 0 & 1 & 1 & \cdots & 1 & 1 \\ 1 & 0 & 1 & \cdots & 1 & 1 \\ \vdots & \vdots & \vdots & \ddots & \vdots & \vdots \\ 1 & 1 & 1 & \cdots & 1 & 0 \\ 0 & 0 & 1 & \cdots & 1 & 1 \\ \vdots & \vdots & \vdots & \ddots & \vdots & \vdots \\ 1 & 1 & 1 & \cdots & 0 & 0 \end{bmatrix} \end{aligned} \tag{18}$$

The green, blue and red blocks denote fault-free, single fault and double fault models respectively. 1 denotes a working sensor that is recording the structural response, contaminated by the sensor noise, while 0 denotes that the sensor at that position is faulty and gives away only sensor noise.

Of course, this approach theoretically prevents the detection of sensor faults occurring at the same time instant which however can be considered not abundantly happening in reality. Nevertheless, such scenarios can be encompassed through further modification of $\mathcal{S}$, yet not considered in this paper for simplicity. Alternate modeling for the fault scenarios and their occurrence can be envisioned. They will generalize this paper without refuting the basics of this approach. An empirical robustness test of this assumption is performed in the numerical simulations.

For the SKF approach, the candidate measurement models, i.e. $\bar{\mathcal{H}}_k^i$ can then be obtained as

$$\bar{\mathcal{H}}_k^i = \mathcal{S}^i \cdot \bar{\mathcal{H}}_k \tag{19}$$

wherein $a \cdot b$ denotes the inner product between a and b. Finally, a suitable assumption has to be made on the model state transition probability $\mathbf{Z}^{ij}$ which is defined as

$$\mathbf{Z} = \left[\begin{array}{c|cccc} \tilde{Z}_0 & \beta & \beta\cdots & \beta & \beta \\ \hline Z_1 & \delta & \cdots & \beta & \beta \\ \vdots & \vdots & \vdots\ddots & \vdots & \vdots \\ \tilde{Z}_1 & \beta & \cdots & \beta & \delta \\ \hline Z_2 & \delta & \delta\cdots & \beta & \beta \\ \vdots & \vdots & \vdots\ddots & \vdots & \vdots \\ \tilde{Z}_2 & \beta & \beta\cdots & \delta & \delta \end{array}\right] \tag{20}$$

In order to interpret this model transition probability matrix $\mathbf{Z}$, the following has to be considered. The green, blue and red blocks are the transition probabilities of each of the models already presented with $\mathcal{S}$ matrix (c.f. Equation 18) in the respective blocks. Accordingly, the transition probabilities for any arbitrary i^{th} sensor fault model listed in the i^{th} row of the $\mathcal{S}$ matrix are given in the i^{th} row of the $\mathbf{Z}$ matrix. Accordingly, $\mathbf{Z}$ is a $(1 + p + C_2^p) \times (p + 1)$ order matrix depicting transition probabilities for $(p+1)$ transition options corresponding to each model. Among the entries, the first entry is always maintained to be the probability of staying at the current model while the remaining are for fault propagation scenarios, except for the entry δ that denotes the probability of repair.

Here, β denotes the probability of getting induced with another sensor fault. Since at any given time, all the sensors are equally likely to get faulty, the probability of switching from the first model to other models (or any model corresponding to fault progression), is considered to be the same, i.e. β. Further, δ denotes minuscule probability of repair and accordingly a small value has been assumed for it implying that a faulty sensor has a minuscule chance of going back to its perfect working condition again. This also allows the fault detection to recover from a possible false alarm.

$\tilde{Z}_0$, $\tilde{Z}_1$ and $\tilde{Z}_2$ are the probabilities of continuing with the same fault-free, single fault or double fault

Algorithm 1 Proposed algorithm.

1: **procedure** SKF($\mathbf{y}_k, \mathbf{Z}, \mathbf{Q}^{\mathbf{u}}, \mathbf{Q}^{\mathbf{v}}, \mathbf{Q}^{\boldsymbol{\theta}}, \mathbf{R}$) ▷ Input, process and measurement noise covariances
2: At $k = 0$ initialize $\{\mathbf{X}^i_{0|0}\}$ and $\{\mathbf{P}^i_{0|0}\}$ with $i = 1$ corresponding to no sensor fault model ▷ Initialization
3: **for** <each k^{th} measurement $\mathbf{y}_k$ with source switch as $\mathcal{S}^i$ at $k-1^{th}$ time step> **do**
4: **procedure** JEKF($\mathbf{X}^i_{k-1|k-1}$,$\mathbf{P}^i_{k-1|k-1}$)
5: **Prediction**: Propagate state and state error covariance, $\mathbf{X}^i_{k|k-1}, \mathbf{P}^i_{k|k-1}$ ▷ see Equation (11)
6: Selection of all possible model transitions $\{ij\}$ (i.e. $\mathcal{S}^i$ to $\mathcal{S}^j$) from the model transition tree ▷ see Figure 1
7: **for** <each possible model transition $\in \{ij\}$> **do**
8: **Innovation and gain**: Compute innovation, $\mathbf{i}^{ij}_k$, and Kalman gain, $\mathbf{K}^{ij}$ ▷ see Equations (11) and (12)
9: **Measurement Update**: Update state ($\mathbf{X}^{ij}_{k|k}$) and state error covariance ($\mathbf{P}^{ij}_{k|k}$) ▷ see Equation (12)
10: **Likelihood estimation**: Estimate the likelihood of the transition mode ij, $\mathbf{L}^{ij}_k$ ▷ see Equation (13)
11: **end for**
12: **end procedure**
13: Obtain the probability for each transition mode $\in \{ij\}$, S^{ij}_k (also w^{ij}) ▷ see Equation (14)
14: Compute weighted estimates for states and its error covariance ($\hat{\mathbf{X}}^i_{k|k}$ and $\hat{\mathbf{P}}^i_{k|k}$) ▷ see Equations (15) and (17)
15: For time step k, position the switch at j corresponding to $max_{1<j<n_o} S^{ij}_k$
16: Reset the destination switch $\mathcal{S}^j$ as source switch $\mathcal{S}^i$ and go back to **line 3** for time instant $k+1$.
17: **end for**
18: **end procedure**

models respectively. Further, ensuring the total sum of probabilities to be unity, the values for these entries can be obtained as the complimentary to the other transition probabilities, i.e.,

$$\begin{aligned} \tilde{Z}_0 &= 1 - p\beta \\ \tilde{Z}_1 &= 1 - \delta - (p-1)\beta \\ \tilde{Z}_2 &= 1 - 2\delta - (p-2)\beta \end{aligned} \tag{21}$$

With this formalism, n_o in Equation (14) is equal to $p + 1$.

The proposed SKF algorithm for simultaneous sensor fault and damage detection is detailed in a pseudo-code in Algorithm 1.

6. Numerical experiment

Numerical experiments on a simplified building model have been performed to check the efficiency of the proposed algorithm. An 8-story building is simplified as a lumped-mass model with 8 dofs, all in the x-direction, cf. Figure 2. Each floor mass is assumed to be equal, i.e., $m_1 = m_2 = \ldots = m_8 = 14KN$. Similarly, all story stiffness values are also assumed to be equal, i.e., $k_1 = k_2 = \ldots = k_8 = 3000KN/m$. The Rayleigh damping model [39] is availed to determine the damping corresponding to the mass and stiffness matrices. The damping ratio is assumed to be 0.02. The external force is modelled as an SWGN of unit variance, $\mathbb{N}(0, 1)$ N, on all its dofs. To obtain the necessary measurement data (acceleration) for the numerical validation, the mechanical system is simulated for 50 s with a sampling frequency of 50 Hz, for all of the forthcoming cases, unless mentioned otherwise. The numerical response is subsequently contaminated with a 1% SNR (signal-to-noise ratio) SWGN process to mimic the real life measurement noise contamination. It is assumed that electrical noises are always present in the sensor, irrespective of sensor's

intended placement. Hence a fault in the sensor (data) is created by replacing the original simulated data with Gaussian noise equivalent to the measurement noise.

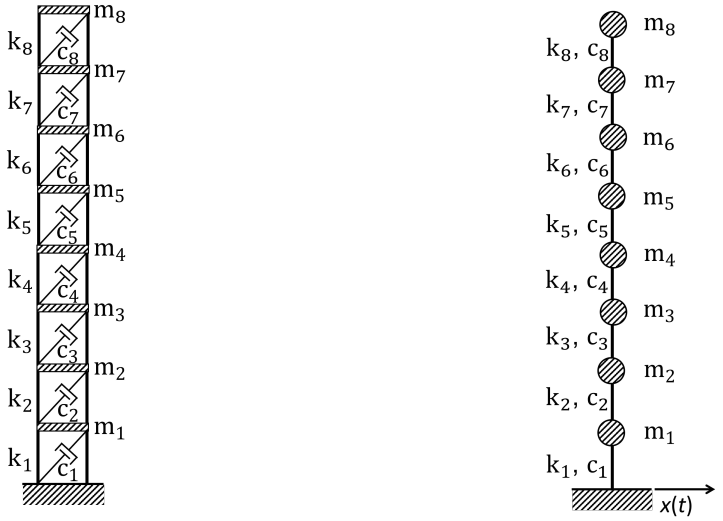

(a) Building model (b) Simplified lumped mass model

Figure 2: Building model for numerical experiments.

6.1. Justification of the requirement of the proposed approach

There exist sufficient studies that demonstrate the capability of JEKF approach in estimating/tracking structural health using a set of measurements. However, the inherent assumption on the quality of measurement is often considered to be too obvious. For cases with faulty sensors, the performance of JEKF can be substantially poor. A numerical experiment is performed on the simplified model (cf. Figure 2), wherein a damage is induced in the third element by a 60% reduction in its stiffness value. Meanwhile, the fifth sensor corresponding to the fifth node of the model is considered faulty, which registers only a Gaussian noise. From past experience with JEKF [40], the state and parameter covariances are selected as, $\mathbf{Q}^{\mathbf{v}} = 10^{10} \times \mathbf{I}$, and $\mathbf{Q}^{\boldsymbol{\theta}} = 10^{3} \times \mathbf{I}$, and have been maintained throughout the article unless mentioned otherwise. However existing methods [41–43] that identify and quantify $\mathbf{Q}^{\mathbf{u}}$, $\mathbf{Q}^{\mathbf{v}}$, and $\mathbf{Q}^{\boldsymbol{\theta}}$ can also be opted.

Figure 3a shows that the JEKF algorithm could not detect the presence of damage in element 3 and wrongly identified damage in fourth and sixth elements which were adjacent to the fifth node/element, where the faulty sensor is assumed. Had the absence of such faulty sensors been supplied to the algorithm, the algorithm could have correctly detected the damage, cf. Figure 3b. Real-life experiments are not immune to such possibility of sensor/s getting faulty during experimentation which justifies the need for a robust approach that can efficiently isolate a faulty sensor and its mal-effects. It should be noted that in the proposed algorithm, JEKF can be substituted by any other damage detection algorithm available, and there should not be any variation in the outcome.

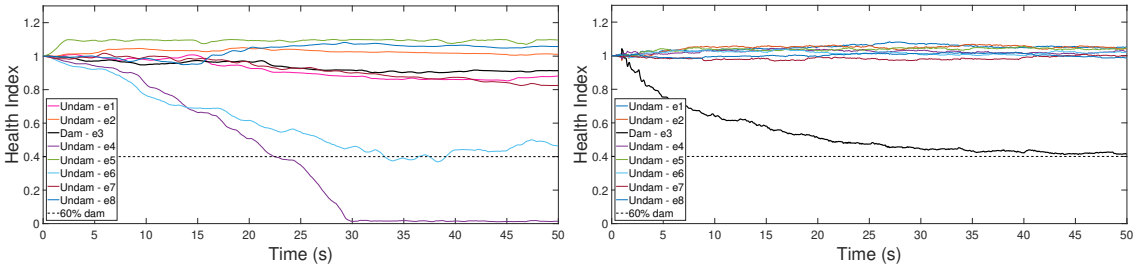

(a) Health Index estimation in the presence of faulty sensor - *faulty sens = 5; dam mem = 3.*

(b) Health Index estimation in the absence of faulty sensor - *faulty sens = none; dam mem = 3.*

Figure 3: Effect of the presence of faulty sensor on Health Index estimation - JEKF.

The proposed method is further investigated for several cases: i) presence of single faulty sensor (Section 6.2), ii) presence of multiple (consecutive) faulty sensors (Section 6.3), and iii) presence of damage in the structure as well as faulty sensor/s (Section 6.4). For each case, it is assumed during estimation that no two sensors/accelerometers can suffer fault occurrence at the same time instant, meaning, the multi-sensor fault situations are realised by assuming the sensors getting faulty in sequence only. Nevertheless, this does not restrict the algorithm to be employed for simultaneous multi-sensor fault scenarios. Under this assumption, the model state transition probability is chosen as per the structure provided in Equation (21), with $\beta = 0.05$, $\delta = 0.005$, and $\tilde{Z}_0$, and $\tilde{Z}_1$, calculated as per Section 5.1. The number of sensors available for measurement (acceleration) has been assumed to be, $p = 8$. Accordingly, $m = (1 + 8 + 28) = 37$ (one no fault, eight single fault and 28 double fault models) has been assumed as the total number of measurement models employed, with $(p + 1) = 9$ options (n_o) available for each model to transit to others (cf. Figure 1). The proposed approach is subsequently employed on the simulated (contaminated) measurements and the most likely model candidates and their transitions are tracked online.

Note that in the following sections the faulty models have been identified and plotted in recurrence. However, the faulty models have been represented based on the information about the faulty sensors. Thus instead of indicating switch position among m numbers of models, the plots present the health state of the sensors by $(p+1)$ sensor health states (0 corresponding to no-fault and subsequent number $\in 1, p$ as damage at that corresponding sensor).

6.2. Detection of faulty sensor

In real-life SHM, a sensor may stop functioning adequately midway into the experiment or right from the beginning. Since SHM utilizes a lot of instrumentation, it is difficult to keep track of such discrepancies. Hence the proposed algorithm is aimed to detect such faulty sensors promptly so that a faulty measurement does not jeopardize the overall monitoring. To mimic the aforementioned scenarios, two cases are simulated, i) a sensor is faulty from the beginning of the simulation (cf. Figure 4a), and ii) a sensor becomes faulty 10 s after the start of the simulation (cf. Figure 4b). While the case study with fault at the beginning

investigates how robust the fault detection is with the proposed method, the second case study investigates a sudden sensor fault scenario and the proposed method's promptness in isolating it.

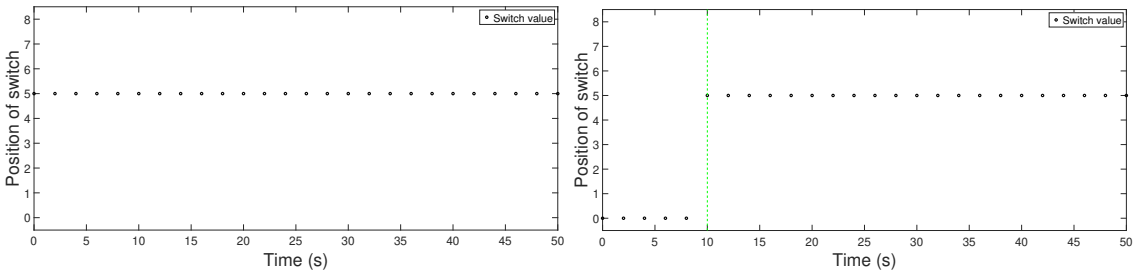

(a) Pre-existing sensor fault (b) Arising sensor fault

Figure 4: Detection of sensor fault - *faulty sens = 5.*

Figure 4 demonstrates the capability of the proposed algorithm in detecting existing as well as sudden faults in the sensors. The detection is perceived to be prompt while being precise with no experience of false alarm (cf. Figure 4b). With the proposed algorithm, the lack of meaningful measurement from the faulty sensor is avoided by selecting suitable measurement model, and thereby estimating corresponding state and parameter. From the estimated states, acceleration data corresponding to the faulty sensor is reconstructed, which had previously registered only noise ($\mathbf{y}_k = \mathbf{H}_k\mathbf{x}_k$, following Equation(4)). Figure 5 demonstrates seemingly accurate acceleration data estimate.

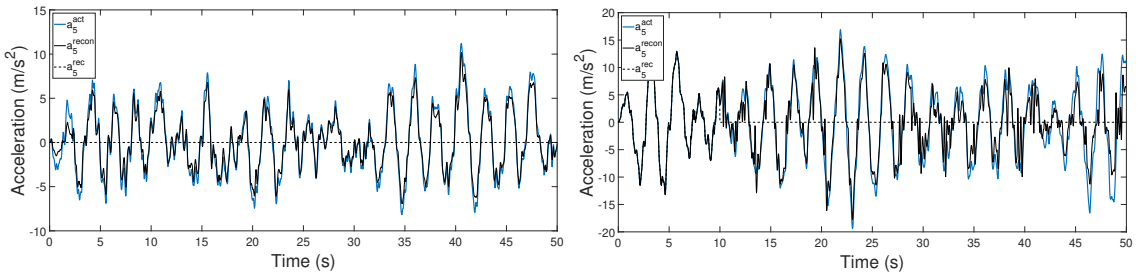

(a) Estimated acceleration - pre-existing sensor fault (b) Estimated acceleration - arising sensor fault

Figure 5: Estimated acceleration corresponding to the faulty sensor - *faulty sens = 5,*
where, a^{act}, a^{recon}, and a^{rec} are the actual, reconstructed, and recorded acceleration, respectively, corresponding to faulty sensor 5.

6.3. Multi-sensor fault detection

To avoid the non-functioning of sensor/s to affect the damage estimation, a general practice is to thoroughly check the correct working of each sensor at the beginning of the monitoring, manually or through an algorithm similar to the procedure detailed in the previous section. Most of the faulty sensors can thus be detected and isolated. Subsequently rectification can be performed before the inspection or the faulty measurement can be allowed to be corrected by the proposed approach. However, it is not rare to find that a second sensor goes faulty even in the presence of a pre-existing faulty sensor. This scenario has already

been discussed previously and can be corrected by altering the candidate model, cf. Section 5.1. The same approach has been employed here for a case study with multi-sensor faults.

For this, the lumped-mass model is simulated with the third sensor getting faulty at 10^{th} s after the start of the simulation. Next, the fifth sensor also gets faulty starting at 20^{th} s of the simulation and thereafter the acquisition system records faulty measurement data from the mentioned sensors till the end of the simulation. Figure 6 shows the capability of the proposed algorithm in detecting multiple consecutive faults in different sensors. With the presumption made within the model switch transition that the probability of a faulty sensor to work again is very low (Section 5.1), the switch transition should be interpreted keeping prior switch position into consideration. The timing in switching the model also describes that the model selection with the proposed algorithm is significantly prompt.

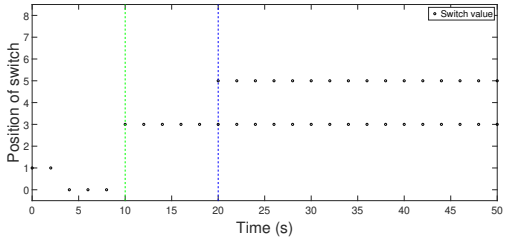

Figure 6: Identification of multiple faulty sensors - *faulty sens = 3 & 5.*

The algorithm has further been successful to reconstruct the acceleration data corresponding to both the faulty sensors 3 and 5, with minimum deviation from the actual acceleration data (except at the crests and troughs) (cf. Figure 7).

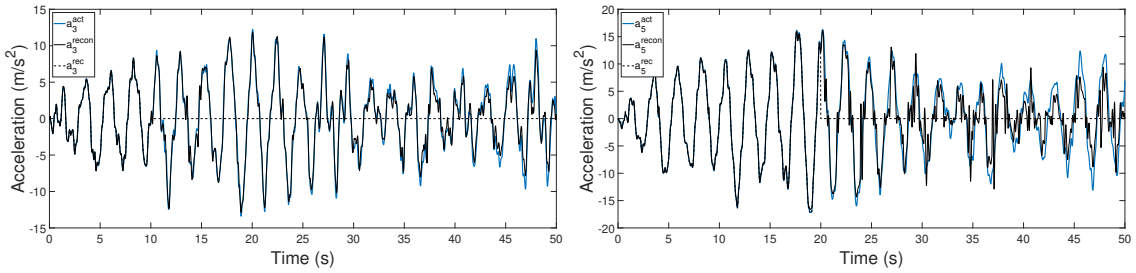

(a) Estimated acceleration corresponding to sensor 3

(b) Estimated acceleration corresponding to sensor 5

Figure 7: Estimated acceleration corresponding to the faulty sensor - *faulty sens = 3 & 5,*
where, a^{act}, a^{recon}, and a^{rec} are the actual, reconstructed, and recorded acceleration, respectively, corresponding to faulty sensors 3 & 5.

6.4. Structural damage identification in the presence of faulty sensor/s

The major objective of this study is to ensure that the presence of some faulty sensor/s does not hinder the functioning of the employed SHM approach. The detection of structural anomalies should ideally be equally seamless regardless of the presence or absence of faults in certain sensors in a network of sensors.

Sensor fault isolation with the proposed algorithm has already been discussed in the previous section. Its efficiency in prompt detection and estimation of structural damage is investigated next. Damage is quantified with the help of **HI**s that quantify location health with values ranging from 0 (complete damage) to 1 (no damage). The model is now simulated for 80 s at 50 Hz sampling frequency with an induced damage and the response is recorded assuming the presence of faulty sensors. A 60% damage is induced in the 3^{rd} member of the lumped-mass model by reducing its stiffness to 40% of its original value. A fault in sensor 5 is induced 1 s after the start of the simulation. The proposed algorithm is subsequently employed with the recorded response to isolate sensor faults while identifying the damage in the structure.

Figure 8 shows that the proposed algorithm is capable of detecting and quantifying damage in the structure as well as identifying and localizing the faulty sensor. The algorithm has correctly identified the presence of fault in sensor 5 immediately after its occurrence (cf. Figure 8a), safeguarding the damage estimation algorithm. An **HI** of about 0.4 is estimated for the third stiffness element that corresponds to the 60% damage induced during the simulation. The proposed algorithm is found to be prompt, precise and efficient in detecting damage in the model (cf. Figure 8b) in the presence of sensor fault.

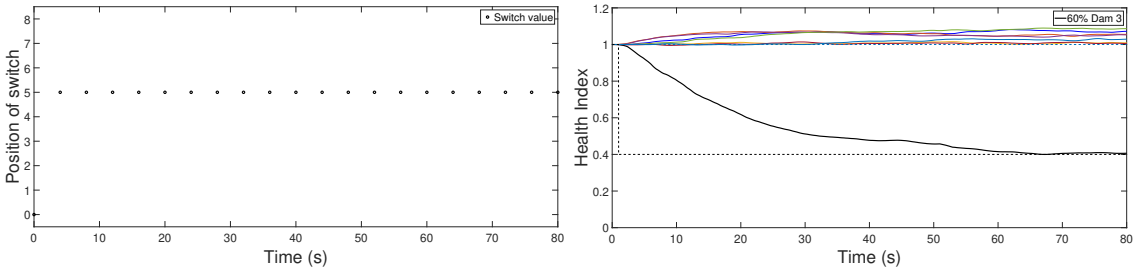

(a) Identification of faulty sensor

(b) Health Index estimation

Figure 8: Detection of faulty sensor and structural damage - *faulty sens = 5; dam mem = 3.*

Further investigation on the performance of the proposed algorithm is undertaken by introducing a 60% damage in the second member with successive faulty sensors. It is assumed that any faulty sensor stays defunct throughout the simulation (cf. Section 5.1). Accordingly, faults in sensors 3 and 5 are introduced 10 s and 20 s after the start of the simulation, respectively. The proposed algorithm is able to detect, localize and estimate the extent of damage present in the structure while promptly isolating both the faulty sensors, cf. Figure 9.

In real-time SHM, a sudden member damage may lead to sensor faults in its vicinity. The proposed algorithm is further tested for its efficacy under simultaneous initiation of sensor fault and member damage. A fault is introduced in sensor 5 while a 60% damage is induced in the 3^{rd} member, after 1 s of simulation. The system is simulated for 120 s. The proposed algorithm (cf. Figure 10) is able to accurately detect presence of sensor fault as well as damage in member. While the sensor fault detection was prompt, the promptness for damage detection decreased when compared to that observed in Figure 8b, where sensor

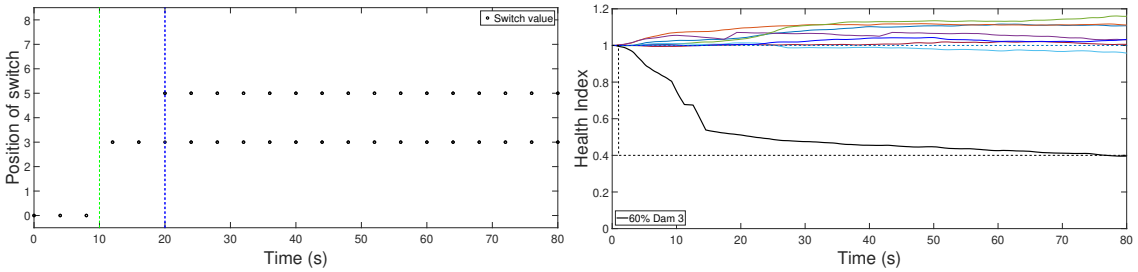

(a) Identification of faulty sensor (b) Health Index estimation

Figure 9: Detection of faulty sensors and structural damage - *faulty sens = 3 & 5; dam mem = 3.*

fault and member damage were initiated at different time instants.

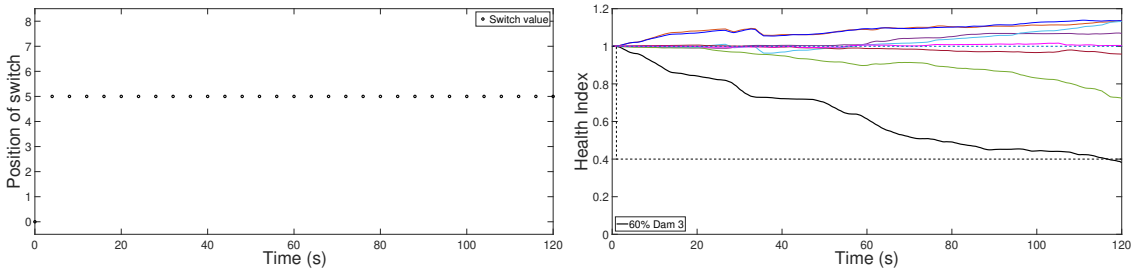

(a) Identification of faulty sensor (b) Health Index estimation

Figure 10: Detection of simultaneous sensor fault and structural damage - *faulty sens = 5; dam mem = 3.*

The proposed algorithm's efficiency is checked under simultaneous initiation of multiple sensor faults (3 and 5) and member damage (60% damage in member 4). The faults and the damage start 1 s into the simulation. Instead of utilizing double fault model from the beginning (Equation (18)), the algorithm follows the same approach as followed in multiple consecutive faults (cf. Figure 9) where the algorithm is started by considering no fault is present, followed by detection of a single fault. If a single fault is detected consistently for certain iterations (here, 1000), the pertinent double fault model is introduced in the algorithm. The iteration number has been arbitrarily chosen, however it is suggested that a minimum of 500 iterations - depending on sampling rate (not more than a few seconds) - maybe considered so that the presence of single fault is ascertained. It is a trade-off to be adjusted by the user. Figure 11a shows that the algorithm detected the simultaneous faults promptly and accurately. Meanwhile damage in member 4 has also been accurately identified. It has also been observed that the promptness in detection of damage with simultaneous multiple fault is slower than that presented in before mentioned cases (Figures 9b and 10b).

To understand the effect of SNR, sensor number and location on the proposed approach, several case studies have been undertaken with a summary of them listed in Table 1. Under these investigations, the third member has been damaged by 30% after 1 s of the start of the simulation and a sensor fault is induced after 15 s. For C.No. 1-4, measurement noise sensitivity studies for noise contamination levels of 1/2/5/10%

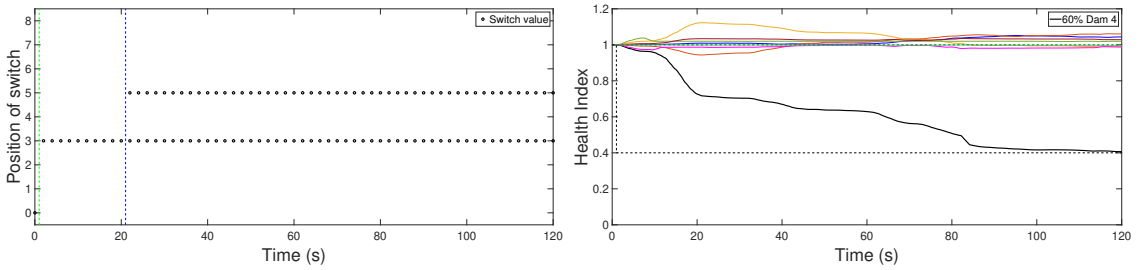

(a) Identification of faulty sensor

(b) Health Index estimation

Figure 11: Detection of simultaneous sensor faults and structural damage - *faulty sens = 3 & 5; dam mem = 4.*

SNR have been undertaken. While the isolation of the faulty sensors has been perceived to be prompt, the accuracy in damage detection has been observed to deteriorate with increasing noise levels.

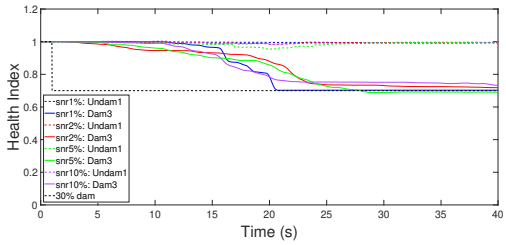

Figure 12: Measurement noise sensitivity - *faulty sens = 5; dam mem = 3.*

Similar measurement noise sensitivity study has been done with a varying number of sensors (cf. Table 1). The accuracy in damage detection has been observed to be dependent on the sensor density besides the noise levels. A few false positives (for member damage) have also been observed for higher SNR% and lower sensor densities. The algorithm fails to correctly determine the damaged member for cases C.No. 11-13. However it should be noted that this inefficiency should be attributed to the intrinsic performance of the damage detection algorithm, here JEKF. Therefore, keeping the complexity level of the problem into consideration, the investigator must choose the proper filter-based damage detection algorithm to couple with the proposed SKF approach.

Table 1: Signal-to-noise ratio, sensor number and location sensitivity.

C.No.	No. of sensors	Sensor fault location - detection	SNR (%)	Damage location - detection	Accuracy (%)	False positive	
						Sensor fault	Member damage
1	8 - {1:8}	5 - ✓	1	3 - ✓	99.61	×	×
2			2		97.60	×	×
3			5		98.10	×	×
4			10		95.28	×	✓
5	6 - {1:6}		1		99.24	×	×
6			2		97.12	×	×
7			5		97.54	×	✓
8			10		94.85	×	✓
9	4 - {1:4}	4 - ✓	1		98.00	×	×
10			2		96.41	×	×
11			5	3 - ×	–	–	–
12			10		–	–	–
13	3 - {1:3}	2 - ✓	1		–	–	–

7. Experimental validation - Cantilever beam

To investigate the performance of the proposed algorithm on real-life structures, a laboratory experiment has been conducted on a cantilever beam (cf. Figure 13a) replicated with a numerical 2D Euler-Bernoulli beam for the proposed model-based damage detection approach. The length of the beam is 750 mm with a cross-sectional area of 8 $mm \times 8$ mm. Further, the numerical model is calibrated (detailed later) for its material properties in order to ensure perfect replication of the real beam. Details of geometric and calibrated material properties are presented in Table 2. The schema of the numerical model compared to the real experiment is presented in Figure 13b.

Table 2: Properties of the cantilever beam.

Length of beam	750 mm
Cross section of beam	8 $mm \times 8$ mm
Calibrated modulus of elasticity	135 GPa
Calibrated density	7890 Kg/m^3
Damping ratio	0.006

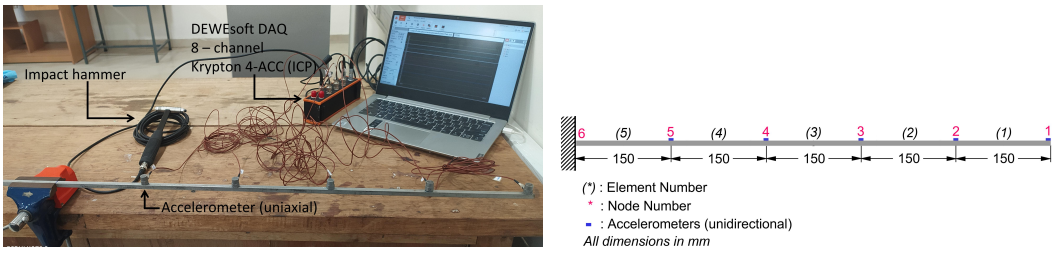

(a) Experimental setup

(b) Schematic numerical model

Figure 13: Experimental setup - cantilever beam.

7.1. Calibration of the numerical model

The experimental beam is segmented into 5 elements and the accelerometers are placed on each of the 5 free nodes (cf. Figure 13b). By parameterizing each of the health elements, isolation of the damage location is possible. The accelerometers are sampled at a fixed sampling rate of 1000 Hz for 3 s. The cantilever beam is subjected to an arbitrary input force by an impact hammer. The measured signal is further decomposed in frequency domain using the frequency domain decomposition (FDD) approach. Figure 14a highlights the first two natural frequencies obtained from the undamaged cantilever beam, (i.e., $\omega_1 = 9.40$ Hz, and $\omega_2 = 56.64$ Hz). The associated frequency response function (FRF) is presented in Figure 14a. The sensors from which the signal for the FDD computation was sampled were all functioning perfectly.

Simultaneously, the supporting numerical FEM model is developed with similar spatial discretization and each of the elements is defined as a 2D-Euler-Bernoulli beam element. The modulus of elasticity (E) and density (ρ) are firstly assumed for the model which is further manually calibrated to obtain a set of

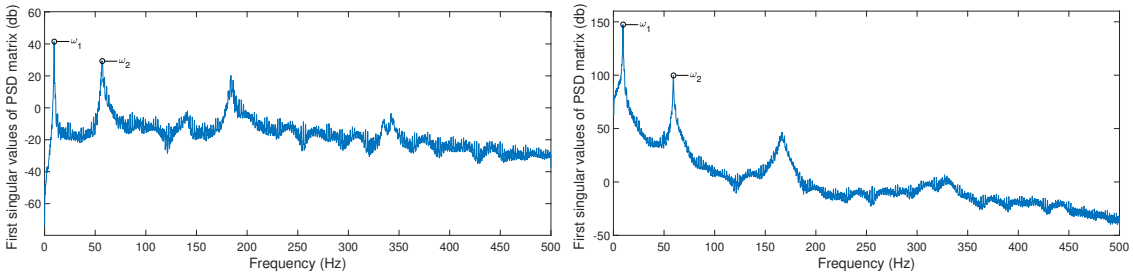

(a) FDD of acceleration data obtained from the experiment; $\omega_1 = 9.40\ Hz$, and $\omega_2 = 56.64\ Hz$

(b) FDD of acceleration data obtained from calibrated numerical model; $\omega_1 = 9.40\ Hz$, and $\omega_2 = 57.33\ Hz$

Figure 14: Calibration of the 2-D cantilever beam by comparing frequencies obtained from Frequency Domain Decomposition (FDD); ω_1, and ω_2 *are the first, and second frequency of the structure, respectively.*

E and ρ that results in a set of natural frequencies that are marginally close (within 1-2%) to the ones obtained experimentally. The calibrated material properties are presented in Table 2. The FRF and the natural frequency peaks for both experimental beam and numerical model are presented in Figure 14. It can be verified that the calibrated numerical model closely replicates the reality. Still, this model assumes the same material properties for all its elements which is not practical for the present purpose.

In the following, the measured response, corresponding to the undamaged cantilever beam and no sensor faults, is processed through the proposed algorithm. Five **HI**s corresponding to the five elements are defined and selected randomly around 1 and further the proposed algorithm is employed to converge to their corresponding best estimates. The model state transition probability is chosen such that $\beta = 0.01$, and $\delta = 0.001$, with $\tilde{Z}_0$, and $\tilde{Z}_1$, calculated following Section 5.1, $m = (1 + 6 + 15) = 22$ and $n_o = 6$. Further, the state and parameter covariances have been tuned to $\mathbf{Q}^{\mathbf{v}} = 10^{-11} \times \mathbf{I}$, and $\mathbf{Q}^{\boldsymbol{\theta}} = 10^{-4} \times \mathbf{I}$ for the current and the following experiments. The convergence of the **HI**s to their respective best estimates are presented in Figure 15a and corresponding elasticity values (pertaining to individual members) are calculated. These values are then selected as the initial healthy state of the respective members for experiments performed in Section 7.2. Meanwhile, the algorithm additionally identified the absence of any faulty sensor, with the switch position consistently at zero for the entire time (cf. Figure 15b). Consequently, this updated model is used as the undamaged predictor model in the proposed algorithm from here on.

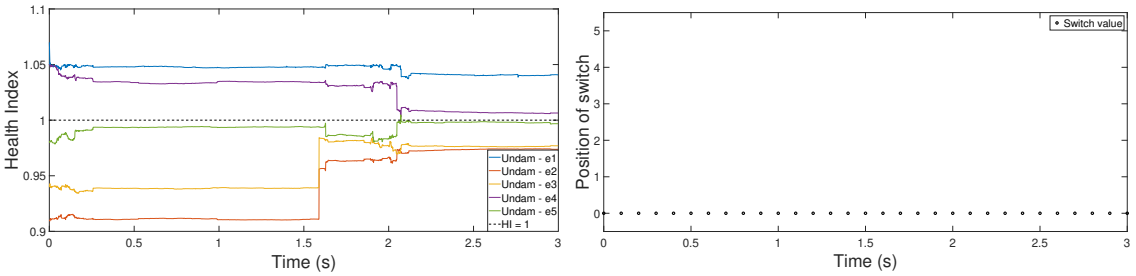

(a) Health Index estimation of the elements, e1-e5.

(b) Identification of faulty sensor by the proposed algorithm.

Figure 15: Bench-marking health indices with respect to undamaged 2-D cantilever beam.

7.2. Experimental verification of the proposed approach

Further experiments are performed on the cantilever beam with sensor faults and damage. In practice, it has been experienced that a sensor fault can be caused by several reasons: sensor detachment, tearing or connection faults in the sensor/data acquisition system (DAS) ends, hardware faults in the response recording channels, etc. Among them, two types of sensor fault scenarios have been considered: detaching the second sensor from its position and loosening the connection of wire of the second sensor to the DAS. It has been observed that for sensor fault scenarios, DAS records only a sensor noise from which measurement noise covariance has been estimated. Similar to the calibration study, the acceleration data is recorded for 3 s at a sampling frequency of 1000 Hz.

A fault is introduced in sensor 2 for the entire duration of the experiment, whereas no damage is inflicted on the cantilever beam. Figure 16a shows that the algorithm is able to detect the faulty sensor (sensor 2) with no false positives. Furthermore, the algorithm correctly established an absence of any damage with the **HI**s for all the members being estimated around their nominal value, i.e. ≈ 1 (cf. Figure 16b).

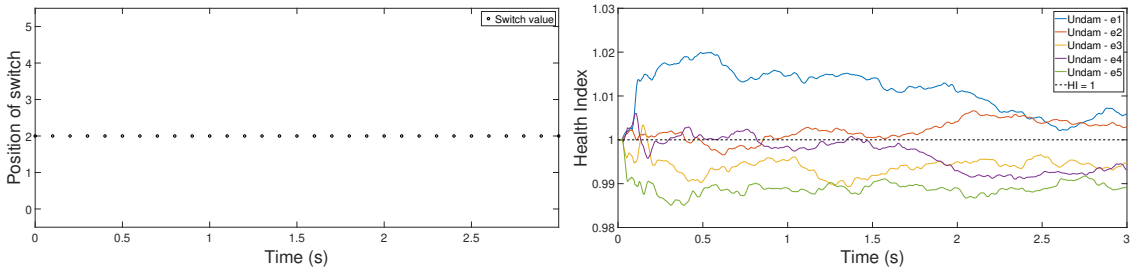

(a) Identification of faulty sensor

(b) Health Index estimation

Figure 16: Detection of faulty sensors and structural damage - *faulty sens = 2; dam mem = none.*

For logistical reasons, the structure was not allowed to be damaged. Therefore, to establish the efficiency of the proposed method in estimating **HI**s, one of the initial **HI**s, i.e., **HI** corresponding to e1 (element 1), is set to 1 with an increased modulus of elasticity, $E = 180\ GPa$. This value is 1.33 times its bench-marked value of 135 GPa, mimicking a 25% damage in element, e1, which is subsequently estimated using the proposed method. A fault in sensor 2 is established for the entire duration. Figure 17 substantiates that the proposed algorithm is capable of identifying the faulty sensor (Figure 17a) as well as detecting damage in the structure in the presence of faulty sensor data (Figure 17b).

8. Conclusion

Sensor faults being inevitable during a real-life structural health monitoring endeavor, it is practical to make the employed SHM approaches robust against such potential sensor faults. In an ideal sense, it is desired that a sudden sensor fault is isolated as soon as it occurs in order to avoid the effects of erroneous measurements which might lead to inaccurate and/or divergent estimates. To fulfil this objective, this paper

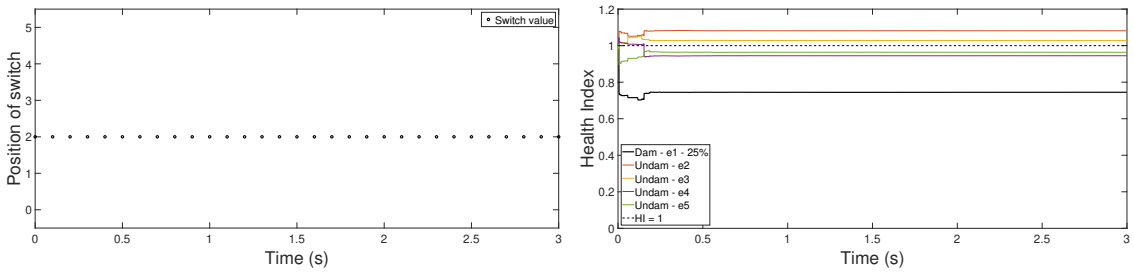

(a) Identification of faulty sensor

(b) Health Index estimation

Figure 17: Detection of faulty sensors and structural damage - *faulty sens = 2; dam mem = 1.*

proposes an Joint Extended Kalman filtering (JEKF) approach coupled with a switching filtering strategy. The switching strategy relies on multiple measurement models corresponding to all possible single fault scenarios, and a switch variable is defined to select the most suitable candidate among all the models. This strategy ensures immediate removal of the measurement sampled at the faulty sensors in order to ensure stable estimation. The capabilities of the algorithm are illustrated through numerical and real experiments in which the proposed algorithm has been perceived to be prompt, accurate, and sufficiently robust to possible false alarms.

Funding: This study was funded by Science & Engineering Research Board (SERB), New Delhi, India, through grant file no. ECR/2018/001464.

References

[1] Swagato Das, P Saha, and SK Patro. Vibration-based damage detection techniques used for health monitoring of structures: a review. *Journal of Civil Structural Health Monitoring*, 6(3):477–507, 2016.

[2] Guillaume Mercère, Laurent Bako, and Stéphane Lecœuche. Propagator-based methods for recursive subspace model identification. *Signal Processing*, 88(3):468–491, 2008.

[3] Ivan Goethals, Laurent Mevel, Albert Benveniste, and Bart De Moor. Recursive output-only subspace identification for in-flight flutter monitoring. In *Proceedings of the 22nd International Modal Analysis Conference (IMACXXII), Dearborn, Michigan*, volume 7, 2004.

[4] Guillaume Mercère, Stéphane Lecoeuche, and Marco Lovera. Recursive subspace identification based on instrumental variable unconstrained quadratic optimization. *International Journal of Adaptive Control and Signal Processing*, 18 (9-10):771–797, 2004.

[5] Hamed Ebrahimian, Rodrigo Astroza, Joel P Conte, and Costas Papadimitriou. Bayesian optimal estimation for output-only nonlinear system and damage identification of civil structures. *Structural Control and Health Monitoring*, 25(4): e2128, 2018.

[6] Dimitrios Giagopoulos, Alexandros Arailopoulos, Vasilis Dertimanis, Costas Papadimitriou, Eleni Chatzi, and Konstantinos Grompanopoulos. Structural health monitoring and fatigue damage estimation using vibration measurements and finite element model updating. *Structural Health Monitoring*, 18(4):1189–1206, 2019.

[7] Subhamoy Sen, Antoine Crinière, Laurent Mevel, Frédéric Cérou, and Jean Dumoulin. Seismic-induced damage detection through parallel force and parameter estimation using an improved interacting Particle-Kalman filter. *Mechanical Systems and Signal Processing*, 110:231–247, 2018.

[8] Subhamoy Sen and Baidurya Bhattacharya. Online structural damage identification technique using constrained dual extended Kalman filter. *Structural Control and Health Monitoring*, 24(9):e1961, 2017.

[9] Hasan Katkhuda, Nasim Shatarat, and Khaled Hyari. Damage detection in steel structures with semi-rigid connections using unscented Kalman filter. *International Journal of Structural Integrity*, 2017.

[10] Jianye Ching, James L Beck, and Keith A Porter. Bayesian state and parameter estimation of uncertain dynamical systems. *Probabilistic engineering mechanics*, 21(1):81–96, 2006.

[11] Alberto Corigliano, Martino Dossi, and Stefano Mariani. Model order reduction and domain decomposition strategies for the solution of the dynamic elastic–plastic structural problem. *Computer Methods in Applied Mechanics and Engineering*, 290:127–155, 2015.

[12] Qiang Li, Ranyang Li, Kaifan Ji, and Wei Dai. Kalman filter and its application. In *2015 8th International Conference on Intelligent Networks and Intelligent Systems (ICINIS)*, pages 74–77. IEEE, 2015.
[13] Masaru Hoshiya and Etsuro Saito. Structural identification by extended Kalman filter. *Journal of engineering mechanics*, 110(12):1757–1770, 1984.
[14] Simon J Julier and Jeffrey K Uhlmann. New extension of the Kalman filter to nonlinear systems. In *Signal processing, sensor fusion, and target recognition VI*, volume 3068, pages 182–194. International Society for Optics and Photonics, 1997.
[15] Stefano Mariani and Aldo Ghisi. Unscented Kalman filtering for nonlinear structural dynamics. *Nonlinear Dynamics*, 49 (1-2):131–150, 2007.
[16] David TB Kelly, Kody JH Law, and Andrew M Stuart. Well-posedness and accuracy of the ensemble Kalman filter in discrete and continuous time. *Nonlinearity*, 27(10):2579, 2014.
[17] Neil J Gordon, David J Salmond, and Adrian FM Smith. Novel approach to nonlinear/non-Gaussian Bayesian state estimation. In *IEE proceedings F (radar and signal processing)*, volume 140, pages 107–113. IET, 1993.
[18] Rodrigo Astroza, Hamed Ebrahimian, Yong Li, and Joel P Conte. Bayesian nonlinear structural fe model and seismic input identification for damage assessment of civil structures. *Mechanical Systems and Signal Processing*, 93:661–687, 2017.
[19] Meriem Zghal, Laurent Mevel, and Pierre Del Moral. Modal parameter estimation using interacting Kalman filter. *Mechanical Systems and Signal Processing*, 47(1-2):139–150, 2014.
[20] Subhamoy Sen, Neha Aswal, Qinghua Zhang, and Laurent Mevel. Structural health monitoring with non-linear sensor measurements robust to unknown non-stationary input forcing. *Mechanical Systems and Signal Processing*, 152:107472, 2021.
[21] He-Qing Mu and Ka-Veng Yuen. Novel outlier-resistant extended Kalman filter for robust online structural identification. *Journal of Engineering Mechanics*, 141(1):04014100, 2015.
[22] Ke Huang and Ka-Veng Yuen. Hierarchical outlier detection approach for online distributed structural identification. *Structural Control and Health Monitoring*, 27(11):e2623, 2020.
[23] Ihab Samy, Ian Postlethwaite, and Da-Wei Gu. Survey and application of sensor fault detection and isolation schemes. *Control Engineering Practice*, 19(7):658–674, 2011.
[24] Kay Smarsly and Kincho H Law. Decentralized fault detection and isolation in wireless structural health monitoring systems using analytical redundancy. *Advances in Engineering Software*, 73:1–10, 2014.
[25] Hai-Bin Huang, Ting-Hua Yi, and Hong-Nan Li. Sensor fault diagnosis for structural health monitoring based on statistical hypothesis test and missing variable approach. *Journal of Aerospace Engineering*, 30(2):B4015003, 2017.
[26] A Rama Mohan Rao, Varun Kasireddy, N Gopalakrishnan, and K Lakshmi. Sensor fault detection in structural health monitoring using null subspace–based approach. *Journal of Intelligent Material Systems and Structures*, 26(2):172–185, 2015.
[27] Xiukun Wei, Michel Verhaegen, and Tim van Engelen. Sensor fault detection and isolation for wind turbines based on subspace identification and Kalman filter techniques. *International Journal of Adaptive Control and Signal Processing*, 24(8):687–707, 2010.
[28] Kevin P Murphy. Switching Kalman filters. 1998.
[29] Lingli Cui, Xin Wang, Yonggang Xu, Hong Jiang, and Jianping Zhou. A novel switching unscented Kalman filter method for remaining useful life prediction of rolling bearing. *Measurement*, 135:678–684, 2019.
[30] Chi Keong Reuben Lim and David Mba. Switching Kalman filter for failure prognostic. *Mechanical Systems and Signal Processing*, 52:426–435, 2015.
[31] Yi-Ming Zhang, Hao Wang, Yu Bai, Jian-Xiao Mao, Xiang-Yu Chang, and Li-Bin Wang. Switching bayesian dynamic linear model for condition assessment of bridge expansion joints using structural health monitoring data. *Mechanical Systems and Signal Processing*, 160:107879, 2021.
[32] Greg Welch, Gary Bishop, et al. An introduction to the Kalman filter. 1995.
[33] Henry Cox. On the estimation of state variables and parameters for noisy dynamic systems. *IEEE Transactions on Automatic Control*, 9(1):5–12, 1964.
[34] Richard E Kopp and Richard J Orford. Linear regression applied to system identification for adaptive control systems. *AIAA Journal*, 1(10):2300–2306, 1963.
[35] Simon S Haykin. *Kalman filtering and neural networks*. Wiley Online Library, 2001.
[36] Zhe Chen et al. Bayesian filtering: From Kalman filters to particle filters, and beyond. *Statistics*, 182(1):1–69, 2003.
[37] Lennart Ljung. Asymptotic behavior of the extended Kalman filter as a parameter estimator for linear systems. *IEEE Transactions on Automatic Control*, 24(1):36–50, 1979.
[38] Steven Reece and Stephen Roberts. An introduction to Gaussian processes for the Kalman filter expert. In *2010 13th International Conference on Information Fusion*, pages 1–9. IEEE, 2010.
[39] Anil K Chopra. *Dynamics of structures, a primer*, volume 2. Earthquake Engineering Research, 1995.
[40] Neha Aswal, Baidurya Bhattacharya, and Subhamoy Sen. Joint and Dual Estimation of States and Parameters with Extended and Unscented Kalman Filters. In *Recent Developments in Structural Health Monitoring and Assessment–Opportunities and Challenges: Bridges, Buildings and Other Infrastructures*, pages 223–252. World Scientific, 2022.
[41] Ka-Veng Yuen and Sin-Chi Kuok. Online updating and uncertainty quantification using nonstationary output-only measurement. *Mechanical Systems and Signal Processing*, 66:62–77, 2016.
[42] He-Qing Mu, Sin-Chi Kuok, and Ka-Veng Yuen. Stable robust extended Kalman filter. *Journal of Aerospace Engineering*, 30(2):B4016010, 2017.
[43] Stefan Wernitz, Eleni Chatzi, Benedikt Hofmeister, Marlene Wolniak, Wanzhou Shen, and Raimund Rolfes. On noise

645 covariance estimation for Kalman filter-based damage localization. *Mechanical Systems and Signal Processing*, 170:
646 108808, 2022.